

Salinity Sensor



Prepared by:

Cameron Clark Department of Electrical Engineering
University of Cape Town

Prepared for:

Justin Pead
Department of Electrical Engineering
University of Cape Town

October 22, 2024

Submitted to the Department of Electrical Engineering at the University of Cape Town in partial fulfilment of the academic requirements for a Bachelor of Science degree in Mechatronics

Keywords: Salinity, Sensor, Conductivity, Temperature, Water, Measurement, Electronics, PCB

Declaration

1. I know that plagiarism is wrong. Plagiarism is to use another's work and pretend that it is one's own.
2. I have used the IEEE convention for citation and referencing. Each contribution to, and quotation in, this report from the work(s) of other people has been attributed and has been cited and referenced. Any section taken from an internet source has been referenced to that source.
3. This report is my own work and is in my own words (except where I have attributed it to others).
4. I have not paid a third party to complete my work on my behalf. My use of artificial intelligence software has been limited to (specify precisely how you used AI to assist with this assignment, and then give examples of the prompts you used in your first appendix).
5. I have not allowed and will not allow anyone to copy my work with the intention of passing it off as his or her own work.
6. I acknowledge that copying someone else's assignment or essay, or part of it, is wrong, and declare that this is my own work



October 22, 2024

Cameron Clark

Date

Acknowledgements

Abstract

Contents

| | |
|---|-------------|
| List of Figures | vii |
| Abbreviations | viii |
| 1 Introduction | 1 |
| 1.1 Problem Statement | 1 |
| 1.2 Background | 1 |
| 1.3 Objectives | 2 |
| 1.4 Scope & Limitations | 2 |
| 1.5 Report Outline | 2 |
| 2 Literature Review | 3 |
| 2.1 Salinity Definitions | 3 |
| 2.2 Salinity Measurement Methods | 4 |
| 2.2.1 Salinity from Chlorinity | 4 |
| 2.2.2 Salinity from Conductivity | 4 |
| 2.2.3 Salinity from Density | 5 |
| 2.2.4 Salinity from Microwave Radiation | 5 |
| 2.2.5 Salinity from Refractive Index | 5 |
| 2.2.6 Salinity from Interferometry | 6 |
| 2.2.7 Salinity from Electromagnetic Induction | 6 |
| 2.3 Salinity Measurement Devices using Conductivity | 7 |
| 3 Theory Development | 8 |
| 3.1 The Calculation of Salinity From Conductivity | 8 |
| 3.2 Electrical Fringing in Conductive Materials | 10 |
| 4 Design | 11 |
| 4.1 Salinity Measurement Method | 11 |
| 4.2 Conductivity Electrode Material | 11 |
| 4.3 Conductivity Electrode Design | 12 |
| 4.4 Resistance Measurement Method | 14 |
| 4.5 Circuit Overview | 14 |
| 4.6 Salinity Calculation and Display | 17 |
| 4.7 Temperature and Depth Measurement | 17 |
| 5 PCB Construction, Adjustments and Code | 19 |
| 5.1 PCB Design | 19 |

| | | |
|----------|---|-----------|
| 5.2 | PCB Adjustments | 20 |
| 5.3 | Probe Code | 21 |
| 5.4 | Controller Code | 23 |
| 5.5 | Board to Board Communication | 23 |
| 6 | Salinometer Evaluation and Testing | 25 |
| 6.1 | DAC Voltage Range and Accuracy | 25 |
| 6.2 | ADC Accuracy | 27 |
| 6.3 | Calibration Resistance | 27 |
| 6.4 | Resistance Measuring Accuracy | 27 |
| 6.5 | Linear Conductivity Measurement | 29 |
| 7 | Conclusions | 32 |
| 8 | Recommendations | 33 |
| | Bibliography | 34 |

List of Figures

| | |
|---|----|
| 2.1 A histogram showing the volume of ocean water relative to temperature and salinity bins. The highest peak corresponds to a volume of 26 million cubic kilometres of ocean water [1]. | 3 |
| 2.2 Global salinity map generated using satellite data [2]. | 6 |
| 2.3 The schematic of a Conductivity, Temperature, Depth (CTD) probe developed by researchers at Uppsala University in Sweden which design contains (a) a temperature sensor, (b) three relatively small electrodes for pH and Cl ⁻ concentration, (c) conductivity electrodes, and (d) a strain gauge for the pressure membrane sensor. The design is $7.5 \times 3.5\text{mm}$ in size [3]. | 7 |
| 4.1 The gold electrode Printed Circuit Board (PCB) design. | 13 |
| 4.2 A simplified representation of the resistance measuring circuit. | 14 |
| 4.3 A simplified representation of the resistance measurement circuit using the gold electrodes with the fringe guard. | 16 |
| 5.1 The probe PCB with the gold electrodes attached and adjustments made | 19 |
| 5.2 The controller PCB with the rotary switch caps attached | 20 |
| 5.3 The flowchart for the probe code that measures salinity. | 22 |
| 5.4 The flowchart for the controller code that communicates with the probe. | 24 |
| 6.1 The input voltage versus the output voltage of the Digital to Analogue Converter (DAC) with no load. | 26 |
| 6.2 The input voltage versus the output voltage of the DAC with a load of 100Ω | 26 |
| 6.3 The voltage output by the DAC measured by a multimeter versus measured by the Analogue to Digital Converter (ADC). | 27 |
| 6.4 The resistance measuring test. | 28 |
| 6.5 The resistance measuring test using the corrected equation. | 28 |
| 6.6 Conductivity test 1 with gold electrodes, the fringe shield, a voltage range of $0 - 2.6V$, and 50 samples taken of salt water sample of unknown | 29 |
| 6.7 Conductivity test 2 with draining and resetting the DAC between each sample. | 29 |
| 6.8 Conductivity test 3 with 25 priming measurements taken before the actual measurement. | 30 |
| 6.9 Conductivity test 4 with a varying number of priming measurements and all true measurement taken as reverse voltage sweeps with 500 samples. | 30 |
| 6.10 Conductivity test 5 with a varying amount of relaxation time before each measurement was taken and 50 samples. | 31 |
| 6.11 Conductivity test 6 with 4 identical tests of 20 samples with 2s of relaxation time between measurements. | 31 |

Abbreviations

%o Parts Per Thousand

ADC Analogue to Digital Converter

CTD Conductivity, Temperature, Depth

DAC Digital to Analogue Converter

DMA Direct Memory Access

EMI Electromagnetic Interference

ENIG Electroless Nickel Immersion Gold

FPU Floating Point Unit

IC Integrated Circuit

LED Light Emitting Diode

PCB Printed Circuit Board

ppm parts per million

PSU Practical Salinity Units

SCB System Control Block

SST Sea Surface Temperature

SYSRESETREQ System Reset Request

UART Universal Asynchronous Receiver-Transmitter

UCT the University of Cape Town

Chapter 1

Introduction

1.1 Problem Statement

There are several methods and designs for measuring salinity. However, none of these are ideal for the challenges faced when measuring the salinity of the ocean beneath the Antarctic ice sheet. Antarctica is the coldest continent on Earth, covered in a vast sheet of ice consisting of around 30 million cubic kilometres in volume, which is about 60% of the world's fresh water [4]. This ice sheet supports a variety of species both above and below it, but the ice itself was thought to be inhospitable to any form of life. However, this has recently been disproven. Small cracks, crevices and pockets in the ice create a habitat for several microorganisms that have adapted to its cold, harsh environment. These microorganisms are the ecosystem's building blocks that survive in and beneath the ice sheet.

Scientists working with the University of Cape Town (UCT) have been studying this unique ecosystem and the physical properties of its habitat to understand how it can thrive in a previously thought lifeless environment. Salinity is one of the physical properties of interest as it typically defines which species can survive in a given environment. *CITE*. The current method of measuring the salinity of the water beneath the ice sheet could be better for several reasons, and a new approach is needed, which this project aims to provide.

1.2 Background

The constant wax and wane of the Antarctic ice sheet creates a unique habitat that supports the microorganisms mentioned above. The ice sheet thickens over time as water accumulates from precipitation, sea spray, and other sources. Salts are also deposited with the water through atmospheric deposition and sea spray. When the water freezes, the salt is expelled into small pockets and channels of highly saline water, known as brine channels.

The brine drains into the ocean, forming a mixture of frigid, saline water and normal seawater, creating a unique environment that could support life. The properties of this mixture of water are not well understood, but they are of interest to scientists studying the ecosystem beneath the ice sheet. Properties in the mixing zone, such as the water's salinity, temperature, currents, light penetration, and more, are all metrics that are currently being investigated.

To measure any given property, an ice core is drilled down to the water's surface, and two main methods are employed to measure the brine-sea water mixture. Either a probe is lowered into the water through the ice core, allowing measurements to be taken at multiple depths, or a sample of the

water is captured by lowering an open canister into the water, closing it at the desired depth, and retrieving it for analysis with hand-held instruments. Salinity is currently being measured using the latter method, which is not ideal. The water sample changes temperature and pressure as it is brought to the surface, which can affect the salinity measurement.

1.3 Objectives

The ideal device is a salinometer with a probe that can be lowered down the ice core to measure the salinity of the water beneath the ice at various depths. However, the aim of this project is to design a prototype, which would aid in investigating its feasibility and establishing a good understanding of the methodology for measuring salinity. This prototype should set the foundation for a future device to be developed that can be used in the field. While the final device needs to be able to perform in the harsh conditions and temperatures of Antarctica, these will only be secondary considerations of this project.

1.4 Scope & Limitations

This project's scope includes the design and development of a prototype device for measuring salinity. This includes researching literature that details similar devices, the theory behind measuring salinity, and the design and development of a prototype device that can test the properties of salt water and lead to a method of measuring salinity. The prototype development also includes testing and evaluating the device to determine its effectiveness in measuring salinity. Additionally, this project should aim to develop the prototype as a separate probe and control unit. The scope does not extend to any development for the final device beyond the prototype nor the analysis of any data captured should the prototype be used in the field.

This project has a budget limitation of R2000 for the entire design, development and testing. This budget can only be spent through [UCT](#) with their approved suppliers and vendors. The project must be completed in 14 weeks from the start to the submission of the final report.

1.5 Report Outline

Lorem ipsum dolor sit amet, consectetuer adipiscing elit. Ut purus elit, vestibulum ut, placerat ac, adipiscing vitae, felis. Curabitur dictum gravida mauris. Nam arcu libero, nonummy eget, consectetuer id, vulputate a, magna. Donec vehicula augue eu neque. Pellentesque habitant morbi tristique senectus et netus et malesuada fames ac turpis egestas. Mauris ut leo. Cras viverra metus rhoncus sem. Nulla et lectus vestibulum urna fringilla ultrices. Phasellus eu tellus sit amet tortor gravida placerat. Integer sapien est, iaculis in, pretium quis, viverra ac, nunc. Praesent eget sem vel leo ultrices bibendum. Aenean faucibus. Morbi dolor nulla, malesuada eu, pulvinar at, mollis ac, nulla. Curabitur auctor semper nulla. Donec varius orci eget risus. Duis nibh mi, congue eu, accumsan eleifend, sagittis quis, diam. Duis eget orci sit amet orci dignissim rutrum.

Chapter 2

Literature Review

2.1 Salinity Definitions

The most commonly understood definition of salinity relates to the total amount of dissolved *salts* in a solution. However, salinity's definition has had several more complex iterations over the last century. One of the first definitions of salinity was the total amount of dissolved *material* in grams in one kilogram of water [5], which is a dimensionless quantity that was expressed in [Parts Per Thousand \(%\)](#) or $g.kg^{-1}$ where most of the ocean water's salinity falls between 34.60% and 34.80% as shown in Figure 2.1 [5].

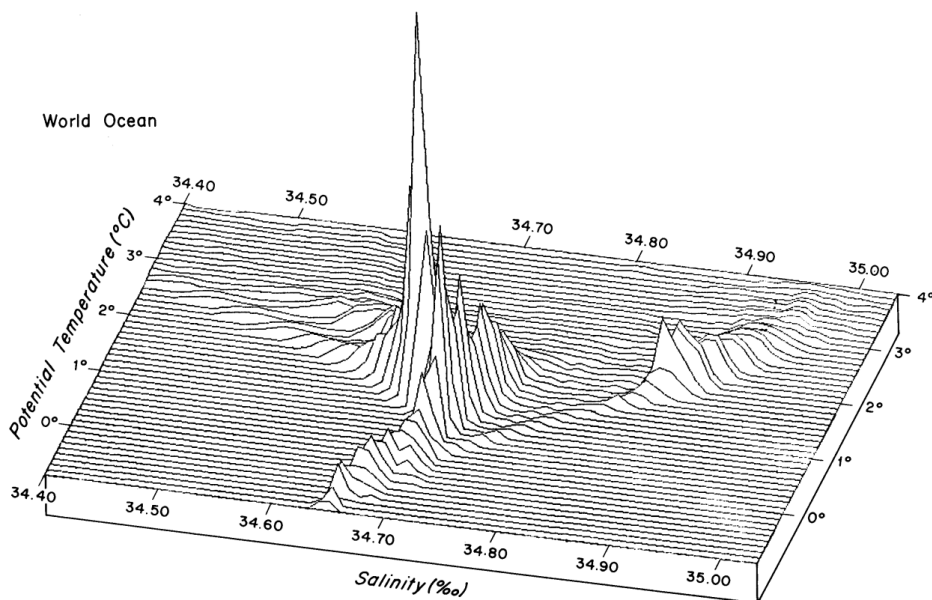


Figure 2.1: A histogram showing the volume of ocean water relative to temperature and salinity bins. The highest peak corresponds to a volume of 26 million cubic kilometres of ocean water [1].

The problem with this definition lay in its testability. Trying to obtain the mass of the dissolved material through evaporation removed certain compounds, making this method inaccurate [6] and other methods of isolating the mass of the dissolved material had similar issues [5]. The need for testability led to salinity being redefined in 1969 to be related to the amount of chlorine present in the water, better known as chlorinity [5]. Chlorinity measurements were well established, and the salinity calculation from chlorinity was relatively simple, which is further discussed in Section 2.2.1.

Around the same time as the salinity-chlorinity relationship was established, oceanographers began experimenting with using conductivity to measure salinity. Conductivity was more precise and straightforward than the titration required to measure chlorinity [7]. In 1978, the Practical Salinity Scale was established, which defined salinity in terms of conductivity and is regarded as the current definition of salinity[7]. While the conductivity measurement was considered easy, the salinity-conductivity relationship was more complex as it had to include corrections for temperature and depth as they both affect the conductivity of an electrolyte solution [8].

The Practical Salinity Scale uses dimensionless units of salinity, which are not interchangeable with \% in the current definition of salinity [9]. Although the Practical Salinity Scale is sometimes given in [Practical Salinity Units \(PSU\)](#), it is more technically correct to refer to it as a certain Practical Salinity ‘on the Practical Salinity Scale PSS-78’ [7]. The salinity calculation from conductivity is further discussed in Section [3.1](#).

2.2 Salinity Measurement Methods

Salinity has had a long history of being measured using various methods with varying degrees of accuracy. Currently, the most common method of measuring salinity is using a [Conductivity, Temperature, Depth \(CTD\)](#) instrument. However, there are multiple alternative methods, most of which have been developed over the last three decades.

2.2.1 Salinity from Chlorinity

The chemical composition of ocean water with a salinity of 35\% contains 19.35\% of Chlorine and 10.77\% of Sodium with the following most common ions only accounting for just above 3\% of the total dissolved solids in the water [10]. This allowed oceanographers to determine that the salinity of ocean water was directly proportional to the amount of chlorine in the water, which holds true provided the ratios of the dissolved materials in the water remained constant. The chlorinity of a solution has an established definition, which was ‘the mass of silver required to precipitate completely the halogens in $0.328\ 523\ 4\text{kg}$ of the ocean-water sample’ [11] which could be tested using titration. In 1969, an accurate relationship between these was established by Reference [11], which was significantly more accurate than the evaporation method achieving accuracies within 0.01\% [6] but was still limited by human error [7].

$$S(\%) = 1.80655 \times Cl(\%) \quad (2.1)$$

2.2.2 Salinity from Conductivity

The conductivity of a liquid is a measure of the ability of the water to conduct an electrical current, which is related to the number of free electrons present in the liquid, which is in turn related to the number of ions present in the liquid [5]. In the case of salt water, the ions present are from the dissolved material, which is what salinity was previously defined on [5]. The relationship between salinity and conductivity accounts for all the ions in the water and thus was considered a more apt measure of salinity [7]. Measuring conductivity was more accurate than titration, achieving accuracies within 0.0002 on the Practical Salinity Scale PSS-78 [12]; automated devices were also able to remove human

error from the measurement [7]. The equation calculating salinity from conductivity, temperature and depth is further discussed in Section 3.1.

2.2.3 Salinity from Density

The density of pure water varies with temperature and is approximately 1000kg.m^{-3} at 4°C [13]. Adding denser materials to the water will intuitively increase its density. This concept is used to determine the quantity of added material using a density measurement, which can be used to calculate salinity [14]. The relationship between salinity and density is approximately linear as shown in Equation 2.2 where ρ is the density of the water, ρ_0 is the density of pure water, k is a proportionality constant, and S is the salinity of the water [15].

$$\rho = \rho_0(1 + kS) \quad (2.2)$$

The more accurate relationship is more complicated and includes a temperature correction defined by Reference [16]. While the accuracy of salinity from density was less than that from conductivity with accuracies within 0.003 on the Practical Salinity Scale PSS-78 [16], Reference [17] still claimed that density was more appropriate to use as the standard potassium chloride solution used to calibrate the CTDs meters did not account for the variation of the ratios of conductive and non-conductive materials commonly present in salt water while the density of the water did.

2.2.4 Salinity from Microwave Radiation

The electromagnetic spectrum interacts uniquely with salt water, scattering, refracting, and reflecting when in contact with it or any material dissolved in it. Different temperature molecules in the water interact with electromagnetic waves differently, and the pressure of the water also varies this interaction. However, the most significant effect is from the presence of the dissolved material [18].

Microwave radiation is one section of the electromagnetic spectrum that can take advantage of this fact to measure salinity [18]. Microwave radiation has a unique advantage as it does not require direct contact with the water to make a measurement, making it possible to measure the salinity of a sample of water from a far distance, including from space [19]. Its advantage necessitated the investigation of the relationship that could accurately predict salinity from a microwave reading [19]. The relationship required multiple different corrections as the microwave readings were found to be affected by Sea Surface Temperature (SST), surface air pressure, surface air temperature, faraday rotation, and surface wind speed [20].

This model has allowed for the development of satellites that can measure the salinity, which has been used to develop global salinity maps as shown in Figure 2.2. The data measured using this method is reported to be accurate to within 0.1 on the Practical Salinity Scale PSS-78 [20].

2.2.5 Salinity from Refractive Index

The second measurement method that takes advantage of the electromagnetic spectrum interaction uses the visible light spectrum to measure the water's refractive index. The relationship between salinity and refractive index is similarly complex, requiring a 27-term equation that includes the effect

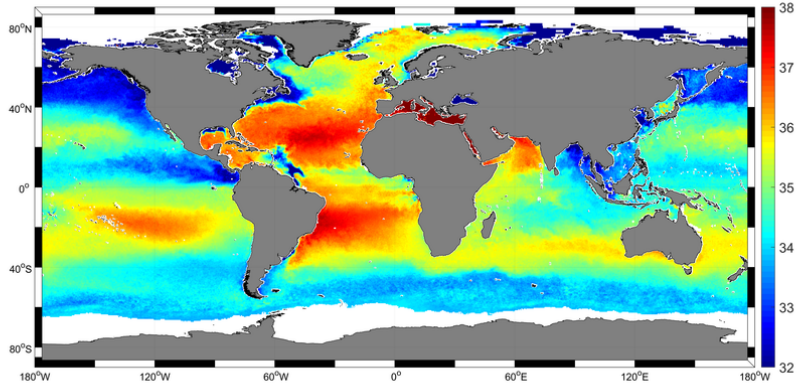


Figure 2.2: Global salinity map generated using satellite data [2].

of pressure and temperature. The refractive index equation is defined a range of $500 - 700\text{nm}$ in wave length, $0 - 30^\circ\text{C}$ in temperature, $0 - 40$ on the Practical Salinity Scale PSS-78, and $0 - 11000\text{dbar}$ in pressure, and it holds an accuracy of $0.4 - 80$ parts per million (ppm) on the Practical Salinity Scale PSS-78, decreasing with increasing pressure. [21]

Refractometers are used to measures the refractive index of water and as only a small amount of the sample is needed, these devices are relatively compact. Two notably compact versions have dimensions of $22.5\text{mm} \times 22.5\text{mm} \times 120\text{mm}$ [22] and $40\text{mm} \times 40\text{mm} \times 70\text{mm}$ [23] which have achieved accuracies of 2 and 83 % on the Practical Salinity Scale PSS-78 respectively.

2.2.6 Salinity from Interferometry

The last measurement method that uses the electromagnetic spectrum is interferometry. Interferometry involves generating two identical light waves on the visible spectrum, passing one through the sample and the other through a non-interfering medium, and then comparing the two waves. The comparative gain and phase shift between the two waves can be used to identify the salinity of a sample of salt water [24].

This method has varying implementations, each with varying results. Reference [25] reported to be accurate within 0.001 on the Practical Salinity Scale PSS-78 using a Michelson interferometer and other researchers have reported other accuracies using different interferometers [26, 27, 28]. The refractometer has the disadvantage of being a large instrument requiring precisely aligned and spaced mirrors to direct the light waves, making it difficult to implement in a compact device.

2.2.7 Salinity from Electromagnetic Induction

Similarly to conductivity, a liquid's magnetic permeability is related to the number of ions present in it. The more ions present in the liquid, the stronger the magnetic alignment that the liquid can generate, increasing its magnetic permeability. In salt water, this is related to the total dissolved solids [29].

Several methods are available for measuring a liquid's magnetic permeability. All involve inducing a magnetic field in the liquid and then measuring its response. These methods all have the advantage of not requiring direct contact with the salt water to make a measurement, which allows for the sample to

remain undisturbed, unlike conductivity and other methods which may be destructive [30]. However, this method has yet to be thoroughly investigated, and the equipment required to measure the magnetic permeability of a liquid is relatively large and has a high power consumption, making it difficult to compact for use in remote environments.

2.3 Salinity Measurement Devices using Conductivity

There are several commercial CTD devices available from small handheld devices such as the [Salinity Pen](#) to large oceanographic research devices such as [Ocean Exploration's CTD](#). These devices are used in various applications with varying prices and accuracies. However, most of their technology is proprietary so the exact workings of their devices are not published.

Some researchers have developed their own CTD devices for specific applications. A study investigating the effect of human activities that alter the salt concentration of water sources such as lakes, ponds and wetlands in Illinois, USA, developed their own CTD. The device reported an average error of 6% in the laboratory validation and 11% in the field validation. It used an alternative approximation of converting the conductivity to salinity, which used single voltage readings to measure the resistance of the water samples, which were then used to create a sensor-specific mathematical model to convert the resistance to salinity [31]. A similar device was shown on a forum with a similar design principle; however, this one was significantly less advanced, making no attempt to correlate the measured resistance values to a salinity value [32].

Researchers at Uppsala University in Sweden developed a nano CTD probe that measured $7.5 \times 3.5\text{mm}$ in size, shown in Figure 2.3. The probe contained everything required for an accurate salinity measurement, and each of the sensors achieved a high degree of accuracy. Unfortunately, the probe's accuracy in calculating salinity was not established; however, this design indicated that miniaturized salinometers are viable and could be used in devices such as bio-loggers on marine animals. [3]

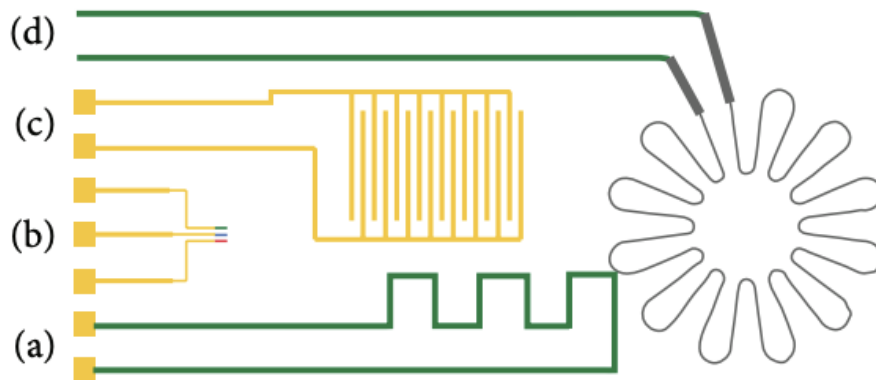


Figure 2.3: The schematic of a CTD probe developed by researchers at Uppsala University in Sweden which design contains (a) a temperature sensor, (b) three relatively small electrodes for pH and Cl⁻ concentration, (c) conductivity electrodes, and (d) a strain gauge for the pressure membrane sensor.

The design is $7.5 \times 3.5\text{mm}$ in size [3].

Chapter 3

Theory Development

3.1 The Calculation of Salinity From Conductivity

Salinity meters that use electrical conductivity are commonly known as [CTDs](#). As depth is a measurement derived from pressure, CTp is the preferred designation when performing calculations [7], which allows for the conductivity of a sample of water to be denoted by $C(S, T, p)$ where conductivity is a function of salinity S , temperature T , and pressure p which is the convention in oceanography [7]. Pressure in the salinity equation is taken relative to sea level where $p = 0\text{dbar}$ is equivalent to an absolute pressure of $P = 101\,325\text{Pa}$ [9]. Using decibars (dbar) for pressure is a common practice in oceanography as it is a unit of pressure roughly equivalent to one meter of water depth [33].

The Practical Salinity Scale defines Practical salinity S_p in terms of a conductivity ratio K_{15} , which is the conductivity of a sample of water at a temperature of 15°C and a pressure equal to one standard atmosphere divided by the conductivity of a standard potassium chloride solution at the same temperature and pressure. The standard potassium chloride solution is 32.4356g of KCl dissolved in 1.000kg of water, and when the ratio between the conductivity of a sample of water and the standard solution, or K_{15} , equals 1, the Practical Salinity S_p is, by definition, 35. [9]

When K_{15} is not equal to 1, the Practical Salinity S_p can be calculated using the PSS-78 equation shown in Equation 3.1.

$$S_p = \sum_{i=0}^5 a_i (K_{15})^{i/2} \quad \text{where} \quad K_{15} = \frac{C(S_p, 15^\circ\text{C}, 0)}{C(35, 15^\circ\text{C}, 0)} \quad (3.1)$$

All the coefficients for the salinity-conductivity equations, including a_i , are given in Table 3.1.

To calculate the salinity of a sample of water that is not at 15°C and 0dbar , the conductivity ratio of the sample can be expanded into the product of three ratios, which are labelled R_p , R_t , and r_t respectively. The conductivity measurement taken in the field $C(S_p, t, p)$ is related to the conductivity of the standard solution $C(35, 15^\circ\text{C}, 0)$ which the device is calibrated with and is represented by R in Equation 3.2. [9]

$$R = \frac{C(S_p, t, p)}{C(35, 15^\circ\text{C}, 0)} = \frac{C(S_p, t, p)}{C(S_p, t, 0)} \cdot \frac{C(S_p, t, 0)}{C(35, t, 0)} \cdot \frac{C(35, t, 0)}{C(35, 15^\circ\text{C}, 0)} = R_p R_t r_t \quad (3.2)$$

check In order to calculate the salinity of the sample, R_t must be found, which takes a similar form to

3.1. The Calculation of Salinity From Conductivity

K_{15} . r_t is first calculated using the temperature of the sample

$$r_t = \sum_{i=0}^4 c_i t^i \quad (3.3)$$

following which R_p is calculated using the sample's pressure p , temperature t and conductivity ratio R ,

$$R_p = 1 + \frac{\sum_{i=1}^3 e_i p^i}{1 + d_1 t + d_2 t^2 + R [d_3 + d_4 t]} \quad (3.4)$$

and finally R_t is calculated using r_t , R_p and R .

$$R_t = \frac{R}{R_p r_t} \quad (3.5)$$

Note that for a sample temperature of $15^\circ C$ and pressure of 0dbar , r_t and R_t both equal 1, which leaves R_t equal to R and thus Equation 3.1 can be used to calculate the Practical Salinity S_p . For temperatures other than $15^\circ C$, the Practical Salinity S_p can be calculated using Equation 3.6 where $k = 0.0162$. [9]

$$S_p = \sum_{i=0}^5 a_i (R_t)^{i/2} + \frac{t - 15}{1 + k(t - 15)} \sum_{i=0}^5 b_i (R_t)^{i/2} \quad (3.6)$$

Table 3.1: Coefficients for the PSS-78 equations [9].

| i | a_i | b_i | c_i | d_i | e_i |
|-----|---------|---------|--------------------------|------------------------|-------------------------|
| 0 | 0.0080 | 0.0005 | $6.766097 \cdot 10^{-1}$ | | |
| 1 | -0.1692 | -0.0056 | $2.00564 \cdot 10^{-2}$ | $3.426 \cdot 10^{-2}$ | $2.070 \cdot 10^{-5}$ |
| 2 | 25.3851 | -0.0066 | $1.104259 \cdot 10^{-4}$ | $4.464 \cdot 10^{-4}$ | $-6.370 \cdot 10^{-10}$ |
| 3 | 14.0941 | -0.0375 | $-6.9698 \cdot 10^{-7}$ | $-4.215 \cdot 10^{-3}$ | $3.989 \cdot 10^{-15}$ |
| 4 | -7.0261 | 0.0636 | $1.0031 \cdot 10^{-9}$ | $-3.107 \cdot 10^{-3}$ | |
| 5 | 2.7081 | -0.0144 | | | |

Note that the coefficients a_i precisely sum to 35 such that the Practical Salinity S_p is 35 when K_{15} or $R_t = 1$ as per Equation 3.1 and Equation 3.6. Additionally, the coefficients b_i precisely sum to 0 such that the Practical Salinity S_p does not depend on the temperature of the water when $R_t = 1$ as per Equation 3.6. [9]

Equation 3.1 to Equation 3.6 are valid for $2 < S_p < 42$ and $-2^\circ C < t < 35^\circ C$ and $0\text{dbar} < p < 10\,000\text{dbar}$ [9]. The range for salinity has been extended using estimations by Reference [34] for $0 < S_p < 2$ and Reference [35] for $42 < S_p < 50$.

The temperatures used in Equation 3.1 to Equation 3.6 are on the IPTS-68 scale [36] and have not been corrected to the currently used ITS-90 scale [37]. In order to correctly calculate the salinity, the temperatures should be converted to the IPTS-68 scale using the equation $t_{68} = 1.00024t_{90}$ before

calculating salinity [37].

3.2 Electrical Fringing in Conductive Materials

Electrical fringing or current spreading, not to be confused with magnetic fringing, occurs when an electrical current flowing through a conductive material spreads like a magnetic field. This is a phenomenon that is particularly prevalent and well studied in the manufacturing of [Light Emitting Diodes \(LEDs\)](#) where the current spreading can be a significant factor in the efficiency of the device [38, 39, 40].

The effect of current spreading in typical conductors is mostly negligible; if the material's conductivity is high enough and its cross-sectional area is small, the current spreading is minimal. However, if a conductor has a significantly larger cross-sectional area than the current requires, such as electrodes in salt water, the current spreading can become a significant factor in its conductivity. This version of current spreading has been studied and is documented for conductors of constant conductivity. [41]

Chapter 4

Design

4.1 Salinity Measurement Method

The industry standard for measuring conductivity is the [CTD](#), which calculates salinity using conductivity, temperature and depth measurement. Section [2.2](#) discussed several alternative methods of measuring salinity. However, most methods have drawbacks that make them difficult or impossible to use in Antarctica.

Refractometers and chlorinity titrations have the same drawbacks as the currently used hand-held [CTD](#), where capturing a water sample and bringing it to the surface alters its temperature and pressure, which may alter its salinity measurement. Microwave radiation has a lower-than-desirable accuracy. In addition, the instruments that measure it, as well as densitometers and interferometers, are expensive and complex beyond the author's expertise. Electromagnetic induction is one of the more promising methods because it is a nondestructive method of measuring salinity, which allows samples to be used for alternative measurements afterwards. However, as mentioned in Section [2.2.7](#), the electromagnetic and salinity relationship has yet to be thoroughly researched, and it requires a high power consumption. This latter is a significant issue in Antarctica as storing power is challenging at very low temperatures, not to mention transporting the device.

The conductivity, temperature and depth method was determined to be the most viable for this project as it is the industry standard, and the author has significant experience with [Printed Circuit Board \(PCB\)](#) design and electronics. Additionally, it has been proven that it can be miniaturized, as mentioned in Section [2.3](#), making it the most likely method to fit through the ice core. This and the other methods face a challenge because the Practical Salinity Scale is not defined for sub-zero temperatures, which may be a problem in Antarctica and should be researched further.

4.2 Conductivity Electrode Material

Ideal electrodes for measuring conductivity in salt water have zero resistance and infinite corrosion resistance and can confine the electrical current in the water to a specific known volume. Electrodes with zero resistance would allow the resistance measured using the electrodes to be entirely due to the water. However, most conductive materials have a conductivity in the order of $10^8 Sm^{-1}$, which causes negligible resistance compared to salt water which has a conductivity range of $0 - 5Sm^{-1}$ [\[42\]](#). The infinite corrosion resistance will allow the electrodes to last indefinitely in the highly corrosive saltwater environment, and several materials with near-perfect corrosion resistance are used in marine

environments, which will be able to satisfy this criterion. The confinement of the electrical current allows for an easier calculation of the conductivity ρ from resistance R if the cross-sectional area A and length l of the water between the electrodes is known as shown by Equation 4.1.

$$\rho = \frac{RA}{l} \quad (4.1)$$

Several materials known for their corrosion resistance include non-precious metals such as aluminium, stainless steel, nickel and copper alloys, and titanium, as well as precious metals such as gold, silver, and platinum. Precious metals are known for having a significantly higher corrosion resistance. However, they are also significantly more expensive.

Choosing the electrode's material involved prioritising high corrosion resistance and low resistance while being restricted to materials that were attainable and within this project's budget. Titanium is the most corrosive resistant of the non-precious metals and has an acceptable conductivity of $2.3 \cdot 10^6$ which is about 25 less than that of copper [43]. Titanium wire was available through off-cuts from a project being conducted by the Chemical Engineering Department of the University of Cape Town. Thus, it was possible to use this material for the electrodes.

Of the precious metals, gold is one of the most accessible as it is a common material used in PCBs manufacturing primarily because of its high corrosion resistance paired with a high conductivity of $49 \cdot 10^6$ which is similar to copper's conductivity [43]. Electroless Nickel Immersion Gold (ENIG) PCB manufacturing is a process where nickel, followed by gold, is deposited onto the copper of the PCB using chemical reactions. While this process is expensive compared to standard PCB manufacturing, it is affordable within this project's budget and made gold a possible electrode material.

Both gold and titanium were used for this project, as they could be manufactured into electrodes of different shapes, which allowed for comparative testing of the materials and the shapes. The electrode design is further discussed in Section 4.3.

4.3 Conductivity Electrode Design

Gold electrodes made using the ENIG PCB manufacturing process were chosen as the device's primary electrodes. The PCB manufacturing process allowed the electrodes to be made with a known area and length of the water between the electrodes, allowing for a more accurate conductivity calculation.

Some scientific papers that attempt to measure salinity are uncertain whether salt water has a constant resistivity relative to the voltage applied. CITE To verify this, the resistance of the water between the electrodes needed to be measured at different voltages while other factors were kept constant, which necessitated close attention to the fringing effect of the electrical current between the electrodes. Thus, wide, flat pads were used on the PCB electrodes, which were placed close together to reduce the current spreading. Additionally, a fringe guard was added to the electrodes, which consisted of a pad that outlined the main conductivity pads that repeated the same voltage as the main pads using an op-amp with unity gain. Ideally, the fringe guard would saturate the volume around the main pads with current and thus prevent them from fringing. This design is shown in Figure 4.1.

The dimensions of the gold electrodes were chosen to be round values, with the pads having a large

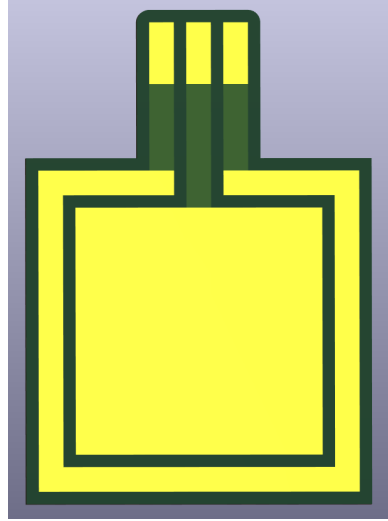


Figure 4.1: The gold electrode [PCB](#) design.

surface area and being placed relatively close together. However, they could not be placed too close together as this could prevent water from effectively flowing between them. Theoretically, this would reduce the proportion of fringing versus linear current between the electrodes. This theory is based on the electrical field fringing effect found in capacitors: take two capacitor pads that are placed close together, which experience a certain amount of fringing; if the area of those two pads increases, the quantity of fringing field will increase relative to the side length while the quantity of linear field which would increase relative to the square of the side length [44, 45].

The second method employed to reduce the fringing effect was to keep the resistance between the pads low, which lowers the voltage required to generate a current through the water, which would theoretically further reduce the current fringing. This theory is also based on capacitors where higher voltages generate stronger electrical fields that spread, or fringe, more.

The gold electrodes were designed with a $20mm \times 20mm$ main pad with a $2mm$ wide fringe guard surrounding it and a spacing between the electrodes of $10mm$. The expected resistance was then calculated to be between 3.75Ω and 6.25Ω using Equation 4.1 and conductivity values for salinities between 40 and 25 on the Practical Salinity Scale PSS-78 [9].

The titanium electrodes were less complicated to design as they only had two variable parameters: their length and spacing. However, as they were made from titanium wire, the fringing effect between them could not be reduced using the same method as the gold electrodes. Thus, it was decided to use the gold electrode to evaluate an accurate method for determining conductivity, which could then be applied to the titanium electrodes, where the fringing effect could be mathematically corrected.

The titanium electrodes are significantly more cost-effective than the gold electrodes. Thus, if an accurate method for determining salinity using them is developed, they will likely become the primary electrodes of the final device. The titanium wire available for this project was $1mm$ in diameter and to account for the unknown resistance between the electrodes, the design allowed for adjustable spacing between the electrodes and adjustable electrode length.

4.4 Resistance Measurement Method

The most common and practical method of measuring resistance is using a resistor divider circuit, which this project chose to employ. While current measuring [Integrated Circuits \(ICs\)](#) exist, the low current ($< 1A$) versions use the same resistor divider principle. Thus, it was considered to be more cost-effective and configurable to design the resistor divider circuit.

The electrodes were chosen to be the R_2 resistor in the voltage divider, and the R_1 resistor was chosen to be a significantly larger, known resistance. The large R_1 value allowed a full range of voltages to be applied to the resistor divider while keeping the voltage across the electrodes low, which was advantageous for the reasons mentioned in Section 4.3. This configuration also prevented the circuit from being short-circuited if the electrodes were to touch, as the R_1 resistor would limit the current. The voltage drop across the electrodes was then amplified using an op-amp to increase the resolution of the voltage measurement.

4.5 Circuit Overview

The resistor divider circuit was designed to be printed onto a [PCB](#) (herewith referred to as the probe) manufactured with [JLCPCB](#). [PCB](#) manufacturing is cost-effective, has a high precision relative to hand soldering, and the process was familiar to the author, making it the ideal method for creating the prototype. However, the resistor divider circuit required a few additions to increase its versatility and testing capability, an overview of which is shown in Figure 4.2.

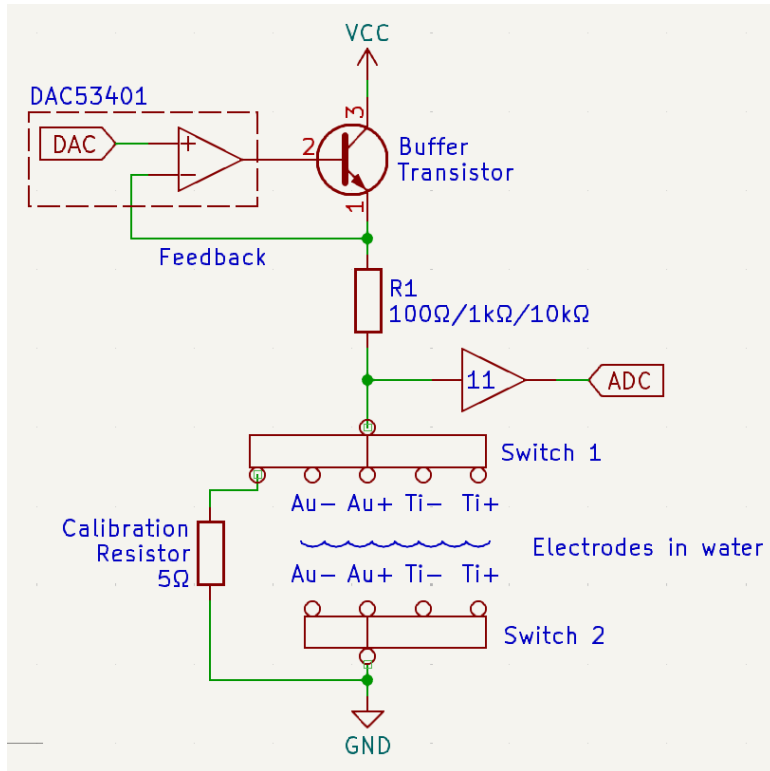


Figure 4.2: A simplified representation of the resistance measuring circuit.

The voltage driving the resistor divider was provided by a [Digital to Analogue Converter \(DAC\)](#) so

that the voltage could be varied and salt water's voltage-resistance relationship could be determined. The **DAC** model was chosen from the **DACs** available on the **JLCPCB**'s website. The model DAC53401 was ultimately chosen for its high updated time of $10\mu s$ and its advanced functionality, which allowed it to output square, triangle, and sawtooth waves. This functionality could be used to perform high-frequency tests in addition to linear voltage sweeps. The **DAC**'s output was connected to the base of a buffer transistor, and its emitter was connected back to the **DAC**'s feedback input. This configuration allowed a higher current to be drawn than the **DAC** could provide while maintaining the specified output voltage.

Sets of switches added to the circuit allowed the voltage produced by the **DAC** to be directed to an R_1 resistor, then across to a pair of electrodes or to a calibration resistor. The switch model TS3A4751 was chosen from **JLCPCB**, which contained four switches in its **IC**, as it was very cost-effective for its low and consistent on-state resistance of around 0.7Ω . The circuit required three switching points: one for choosing the R_1 resistor, one for choosing the anode and one for choosing the cathode.

It was decided to give the R_1 resistor alternate resistances to allow for any possible resistance between the titanium electrodes or unforeseen errors. The R_1 value chosen to pair with the gold electrodes was 100Ω as it was the smallest e12 series resistance that would prevent the board from drawing too much current and burning out the traces or switches. The final resistances were chosen to be 100Ω , $1k\Omega$ and $10k\Omega$, which would be used when the resistance between the probes was $1\Omega - 10\Omega$, $10\Omega - 100\Omega$ and $100\Omega - 1k\Omega$ respectively. This configuration allowed for a minimum resolution of 11% of V_{DAC} for the voltage measurement by the **Analogue to Digital Converter (ADC)** as shown by Equation 4.2.

$$\frac{1\Omega}{1\Omega + 100\Omega} * V_{DAC} * 11 = 11\%V_{DAC} \quad (4.2)$$

$$\frac{10\Omega}{10\Omega + 100\Omega} * V_{DAC} * 11 = 100\%V_{DAC} \quad (4.3)$$

The anode switch (switch 1) allowed R_1 to be connected to any of the four electrodes or to the calibration resistor of 5Ω , and the cathode switch (switch 2) allowed any electrode to be connected to ground. An example of measuring the resistance between the titanium electrodes would be to connect switch 1 to Ti+ and switch 2 to Ti, allowing the voltage drop to be measured. This configuration also allows current to flow in both directions between electrodes, which can prevent an excessive buildup of chlorine gas or sodium electroplating on the electrodes or electrolysis of the water by taking a resistance measurement in both directions in rapid succession.

To increase the accuracy of the R_1 resistors, they were made by placing multiple high-accuracy resistors in parallel, which decreases their resistance uncertainty. The total uncertainty of the parallel resistance $\delta_{R_{total}}$ is decreased by a factor equal to number of parallel resistors n compared to each resistance's

uncertainty δ_R as shown by Equation 4.4 to Equation 4.6.

$$R_{total} = \left[\sum_{i=1}^n \frac{1}{R_i} \right]^{-1} = \left(\frac{n}{R} \right)^{-1} = \frac{1}{n} \cdot R \quad (4.4)$$

for a function $f(x_1, x_2, \dots, x_n)$, its tolerance $\delta_f = \sqrt{\sum_{i=1}^n \left(\frac{\partial f}{\partial x_i} \delta x_i \right)^2}$ (4.5)

$$\therefore \delta_{R_{total}} = \sqrt{\left(\frac{\partial R_{total}}{\partial R} \delta R \right)^2} = \sqrt{\left(\frac{1}{n} \delta R \right)^2} = \frac{1}{n} \delta_R \quad (4.6)$$

The R_1 resistors were made from 3 parallel resistors, each with tolerance $\pm 1\%$ giving a total tolerance of $\pm 0.3\%$ and the calibration resistor was made from 4 parallel resistors with tolerance $\pm 1\%$ giving a total tolerance of $\pm 0.25\%$.

One last switch point was added to the circuit for the gold electrode's fringe guards, an example of which is shown in Figure 4.3. The voltage from R_1 was routed to a buffer op-amp with unity gain. Its output was then connected to the fringe guard, which effectively repeated the same voltage as the main pad while not affecting any measurements using them. The other fringe guard could be switched to ground, allowing a current to be generated between the two. This current would ideally absorb any possible fringing from the main pads. The same switch point also allowed the fringe guards to be electrically disconnected to test their effectiveness and to determine if they interfered with the measurement. Lastly, as the fringe guards held the same voltage difference as the main pads and, in theory, had a higher resistance due to their smaller area, the current flowing between them was assumed to be less than that of the main pads; thus, there was no need to limit the current from the op-amp.

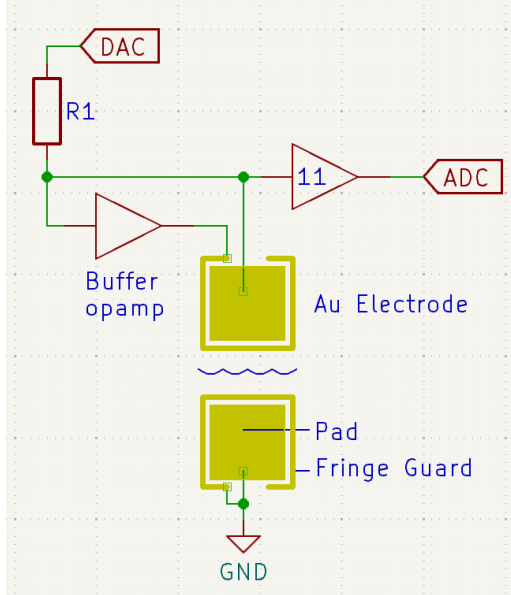


Figure 4.3: A simplified representation of the resistance measurement circuit using the gold electrodes with the fringe guard.

4.6 Salinity Calculation and Display

In order to measure the salinity of the water, the probe [PCB](#) would be lowered through the ice core hole into the water to capture salinity readings at various depths. The measurements could either be captured automatically at preprogrammed depth or time intervals or triggered by the user using a controller. The latter method was chosen for this project because it is a more user-friendly approach, allowing researchers to control precisely which depths the salinity measurements are made and giving them live updates about the probe's status and onboard sensors.

The controller was a straightforward [PCB](#) with input buttons and rotary switches, two 7-segment displays, a [Recommended Standard #485 \(RS-485\)](#) communication port and a simple microcontroller.

Saltwater has a high [Electromagnetic Interference \(EMI\)](#), which interferes with all wireless communication [?]. While high-power wireless communication is viable for ranges up to 70m, it is more reliable, cost-effective, and power efficient to use a wired connection [?]. [RS-485](#) is a robust, long-range embedded communication protocol that only requires a simple [IC](#) to use, making it ideal for this project. Additionally, the author was familiar with this protocol and had previous board-to-board communication experience with it.

[Universal Asynchronous Receiver-Transmitter \(UART\)](#) to [RS-485](#) converters are common as most microcontrollers have a [UART](#) communication port. This project used half-duplex [RS-485](#) as it is the industry standard, and it is more cost-effective than full-duplex [RS-485](#), which requires an additional [UART](#) to [RS-485](#).

The microcontroller was chosen from the STM32F030 series as it did not need to perform any complex calculations, and the author was familiar with this series.

With an external controller, a waterproofed probe could be lowered into the water to measure its salinity. The chosen method of waterproofing the probe was to coat it with epoxy resin, as this was the most familiar and cost-efficient method available. The other notable option is to create a waterproof housing for the probe, but this can be complex and expensive. In addition to the circuitry shown in Figure 4.2, the probe had a temperature and depth sensor, which are discussed in Section 4.7, an [RS-485](#) communication port and a microcontroller. The microcontroller was chosen from the STM32F4 series as it is the most cost-effective series with a [Floating Point Unit \(FPU\)](#), allowing the full salinity calculation to be performed on the probe.

4.7 Temperature and Depth Measurement

Waterproof depth sensors were too expensive for this project's budget, costing around \$100. An alternative approach is to use a non-waterproof pressure sensor that is isolated from the water using a flexible membrane that allows the external pressure to be transmitted to the sensor. The WF183DE pressure sensor was chosen as it was the most cost-effective sensor rated for above 50 meters of water pressure available at [JLCPCB](#). Should this approach fail, the backup plan was to use the controller to manually input a depth so that the salinity could still be calculated.

The temperature sensor was an arbitrarily chosen surface-mount sensor with high accuracy of $\pm 0.3^{\circ}\text{C}$

4.7. Temperature and Depth Measurement

and a wide temperature range of $-45 - 130^{\circ}\text{C}$. Epoxy resin is a poor thermal conductor [?]. Thus, the temperature sensor should be coated with a very thin layer of epoxy when the probe PCB is cast, allowing for a more accurate measurement. The choice of microcontroller and pressure sensor also provided this board with two alternative temperature sensors, which were less accurate but could be used in the event that the primary temperature sensor failed.

Chapter 5

PCB Construction, Adjustments and Code

5.1 PCB Design

The circuits for the probe, controller and gold electrode PCBs were designed using KiCad and manufactured with JLCPCB. The gold electrodes was trivial, only requiring a single layer PCB with pads and traces.

The probe PCB was more complex, fabricated on a 4-layer PCB which is shown in Figure 5.1. JLCPCB offered a discount for 4-layer PCBs that were less than $50 \times 50\text{mm}$ in size which what the dimensions of the probe PCB were. While the probe should ideally be as small as possible to fit through the ice core, the probe was not designed smaller than $50 \times 50\text{mm}$ to allow for an easier debugging process.

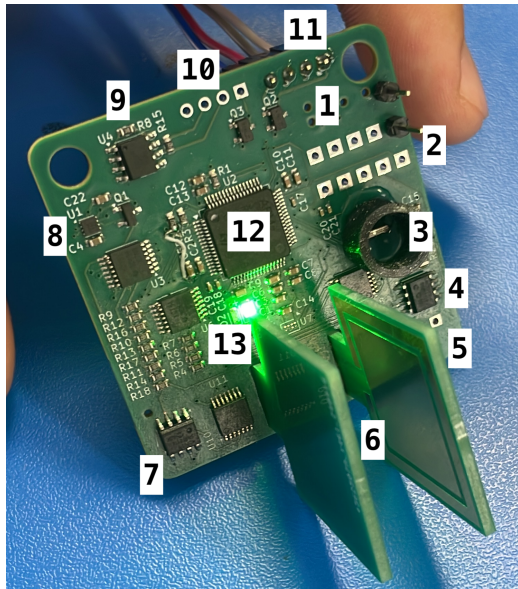


Figure 5.1: The probe PCB with the gold electrodes attached and adjustments made

Table 5.1: Figure Key

| | |
|----|---|
| 1 | Programmer Port |
| 2 | Test Points |
| 3 | Pressure Sensor in a Protective Housing |
| 4 | 11× Gain Op-Amp |
| 5 | Titanium Electrode Port |
| 6 | Gold Electrodes |
| 7 | Unity Gain Buffer Op-amp |
| 8 | DAC and Buffer Transistor |
| 9 | UART to RS-485 Converter |
| 10 | RS-485 Port |
| 11 | UART Port |
| 12 | STM32F4 Microcontroller |
| 13 | LEDs |

Note 1: The rest of the titanium electrode ports are behind the gold electrode.

Note 2: The other ICs present are the switches.

The probe was designed with the resistance measuring circuitry, temperature and pressure sensors,

microcontroller, [UART](#) to [RS-485](#) converter and [RS-485](#) port mentioned in Chapter 4. The gold and titanium electrodes were given ports at the bottom of the board such that they sat perpendicular to the board which was deemed the easiest method of attachment. A [UART](#) port was added next to the [RS-485](#) port to allow for debugging and testing of the probe without the controller. Both of these ports were also made with reverse polarity protection to prevent unintentional damage to the board. Lastly, [LEDs](#) were added next to the microcontroller and a programmer port and test points were added at the top of the board to allow for easy debugging and testing of the board. Having the programmer and communication ports at the top of the board allowed the lower half of it with the probes to be submerged while still being able to communicate with the board.

The controller [PCB](#) was fabricated on a 2-layer board, which is shown in Figure 5.2, as the components were too large to fit on a $50 \times 50\text{mm}$ 4-layer board. [JLCPCB](#) offered a similar discount for 2-layer [PCBs](#) that were less than $100 \times 100\text{mm}$ which is what the dimensions of the controller were restricted to. Ultimately, the dimensions were made to be $100 \times 60\text{mm}$ as this area could comfortably fit all the components.

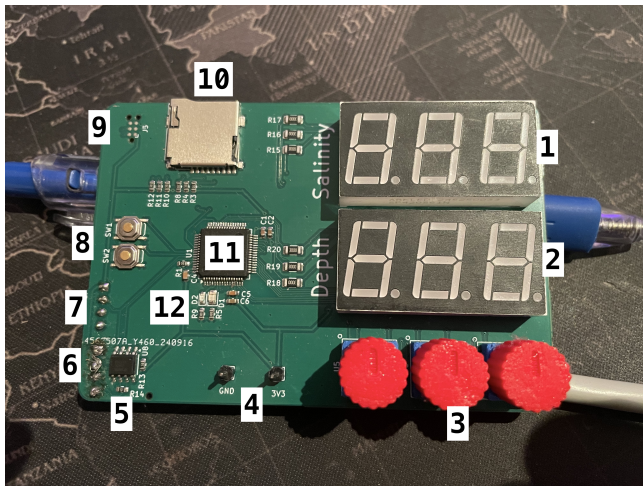


Figure 5.2: The controller PCB with the rotary switch caps attached

Table 5.2: Figure Key

| | |
|----|--|
| 1 | SD Card Port |
| 2 | Salinity 7-Segment Display |
| 3 | Depth 7-Segment Display |
| 4 | Rotary Switches |
| 5 | Power Input |
| 6 | UART to RS-485 Converter |
| 7 | RS-485 Port |
| 8 | UART Port |
| 9 | Input Buttons |
| 10 | STM32F0 Microcontroller |

The controller was designed with the rotary switches, 7-segment displays, [UART](#) to [RS-485](#) converter and [RS-485](#) port mentioned in Chapter 4. The 7-segment displays were designated a default of displaying the salinity and depth of the water using silkscreen, but they could be changed to display anything using software. The components were placed in a user-friendly manner allowing for easy use of the buttons and rotary switches. Similarly to the probe, [LEDs](#), a [UART](#) port and a programmer port added to the board to allow for debugging and testing of the board. It should be noted that an SD Card Port was added for future expansion but was not used nor tested during this project.

5.2 PCB Adjustments

There were three adjustments made to the probe [PCB](#) to ensure that it was functioning as expected excluding the soldering of the headers and gold electrodes. Firstly, one of the pins of the microcontroller was incorrectly not connected to power and was corrected by soldering a wire to connect it to power

which can be seen of the left of the microcontroller. Secondly, the footprint of the pressure sensor was flipped horizontally which was corrected by flipping and soldering the depth sensor vertically. A protective case was added around the pressure sensor to prevent it from being damaged during testing and the casing would also later function as the support for the waterproof membrane that would create the pressure seal.

Lastly, both op-amps were incorrectly chosen and thus had to be replaced with new op-amps that shared the same footprint. The temperature sensor also had an incorrect footprint, but this was not able to be rectified as this was discovered after the board had already been manufactured, and thus the temperature sensor was not soldered to the board. The pressure sensor's onboard temperature sensor was used instead.

The controller [PCB](#) required no adjustments as the design was simple, and the components were all correctly placed. There was one minor error with pin assignments with the rotary switch pins, but this was corrected in software and did not require any hardware changes. Switch caps for the rotary switches were 3D printed and attached to the shafts of the rotary switches to make them easier to turn and to make the controller more user-friendly. It should be noted that the SD Card Port was added for future expansion and was not used nor tested during this project.

5.3 Probe Code

The major steps in measuring salinity are to measure the conductivity of the water between the electrodes, measure the temperature and pressure of the water and then calculate the salinity. An overview of this process along with the process for each major measurement is shown in Figure 5.3.

The conductivity measurement and calculation is different depending on if the voltage-resistance relationship is constant or not which is expected for the gold and titanium electrodes respectively. Both variations start with a voltage sweep where the voltage is increased from the minimum to the maximum voltage with a set voltage step or vice versa by the [DAC](#). At each step, the voltage output of the [DAC](#), the voltage across the calibration resistor and the voltage across the electrodes are measured.

If the ratio between the [DAC](#) voltage and the voltage across the electrodes is not constant, the conductivity will have to be determined by performing tests to create a model that can relate a set voltage samples to a conductivity.

If the ratio between the [DAC](#) voltage and the voltage across the electrodes is constant, the resistance between the electrodes can be calculated using the calibration resistor. Given that the calibration resistance and R_1 is known, the resistance between the electrodes can be calculated for each voltage sample using the ratio between the electrode and calibration voltages as shown in Equation 5.1. k is calculated using the known values V_{ratio} , R_1 and $R_{calibration}$ to simplify the equation as shown in

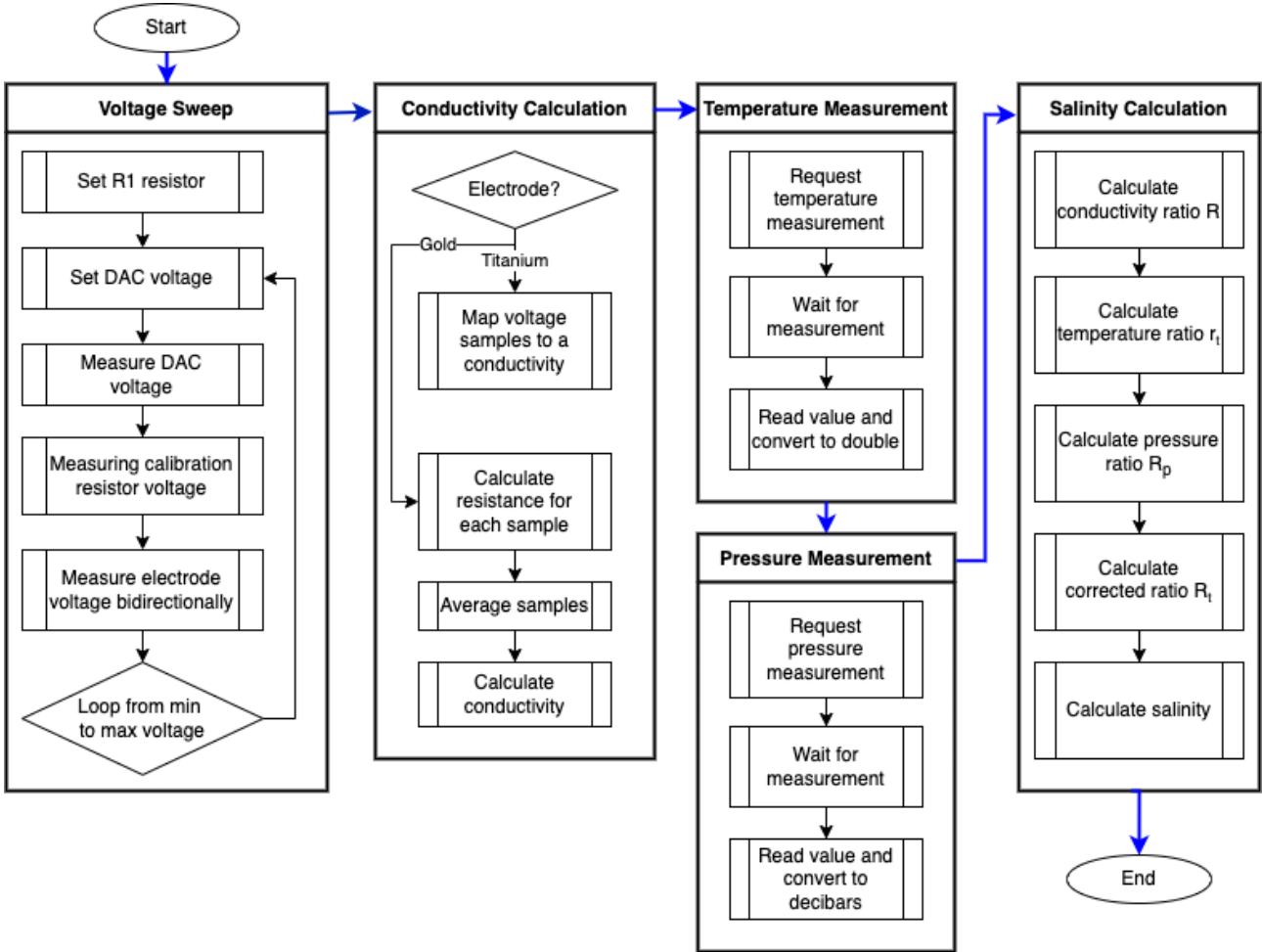


Figure 5.3: The flowchart for the probe code that measures salinity.

Equation 5.2 and finally $R_{electrode}$ can be calculated using Equation 5.3.

$$V_{ratio} = \frac{\frac{V_{DAC}A_{11}A_{ADC}}{R_1 + R_{electrode}}}{\frac{V_{DAC}A_{11}A_{ADC}}{R_{calibration}}} = \frac{\frac{R_{electrode}}{R_1 + R_{electrode}}}{\frac{R_{calibration}}{R_1 + R_{calibration}}} \quad (5.1)$$

$$\frac{R_{electrode}}{R_1 + R_{electrode}} = V_{ratio} \frac{R_{calibration}}{R_1 + R_{calibration}} = k \quad (5.2)$$

$$R_{electrode} = \frac{kR_1}{1 - k} \quad (5.3)$$

The resistance can then be averaged and the conductivity can be calculated for the gold electrodes using Equation 4.1. Using this method allows for the device to nullify all scalar inaccuracies in the circuit including R_1 uncertainty, **DAC** and **ADC** gain errors, and the op-amp gain error as they will all be present in the calibration resistor and the electrodes measurements. This method is however still vulnerable to offset inaccuracies including **DAC** and **ADC** offset errors and the internal resistance of the switches and traces.

Measuring the temperature and pressure is a simple matter of reading the temperature sensor and the pressure sensor respectively which finally allows salinity to be calculated which can be performed on the salinometer microcontroller as it possesses an **FPU**. Additionally, any of the temperature,

depth, resistance or conductivity measurements can be calculated individually and transmitted to the controller if requested.

5.4 Controller Code

For the prospective user, the controller's primary function is to instruct the probe to take a measurement and then to display said measurement, but for the purpose of testing and investigation, the controller was given additional functionality. The main functions of the controller are to instruct the probe to take a measurement, to display the measurement, and to allow for configuration of the probe.

The display was done using 7-segment displays to display the various measurements. Each digit of the 7-segment display was written to by writing the 7-segment digit code and keeping the corresponding digit's cathode low while keeping the others high. This was repeated for each digit in quick succession using timer controlled [Direct Memory Access \(DMA\)](#) to give the illusion of all digits being on at the same time.

The left most rotary switch was used to navigate the menu. The menu included the default of showing both salinity and depth, showing individual measurements of temperature, depth, resistance, conductivity and salinity, and the configurable parameters of the probe. The menu names were displayed on the top row of the 7-segment display and the selected menu item was displayed on the bottom row. This created some limitations on what could be displayed, for instance the best display of temperature was 'teP', but all menu items were still reasonably clear.

When the user selected a measurement menu item, the top switch was configured to request that measurement from the probe and display it and when the user selected the configuration menu item, the top switch was configured to update the probe's configuration. The other two rotary switches were used to adjust the configurable parameters of the probe which are discussed further in Section 5.5. The bottom switch was configured to reset the probe and the controller should an error occur.

5.5 Board to Board Communication

The probe and controller communicate using half-duplex [RS-485](#) communication which is buffered on both sides by the [UART](#) to [RS-485](#) converter. This makes the protocol effectively half-duplex [UART](#) communication from the perspective of the microcontrollers. The probe was configured to be in receive mode where it would be perpetually waiting for a 1 byte command from the controller. All the possible commands and expected responses are shown in Figure 5.4.

While not directly available to the user, the controller can request a status byte to which the probe will respond with *idle*, *busy* or *error* depending on the state of the probe. This allows for some simple error checking and communication flow which could be integrated into more robust error handling in the future. When the user requests a measurement, the controller sends the corresponding request command to which the probe will respond with the measurement data.

When the user requests a configuration update, the controller transfers a configuration packet through the predefined manner shown in Figure 5.4. Once the probe is fully cast in epoxy resin, the configuration

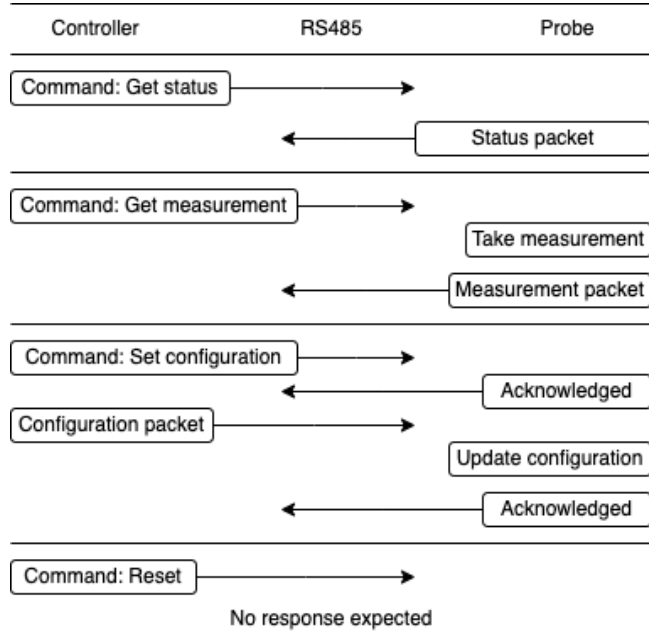


Figure 5.4: The flowchart for the controller code that communicates with the probe.

can only be updated this way so all possibly useful, configurable parameters were included in the configuration packet. This includes which electrode to use (including whether to use the fringe shield or not), the R_1 resistor to use, the directionality of the resistance measurement (unidirectional or bidirectional), the voltage sweep start, end and number of steps among other parameters. Some parameters such as the directionality are unlikely to be changed from their default value (bidirectional) but were included to cover any unforeseen circumstances.

When the user resets the boards using the bottom switch of the controller, the controller first sends a reset command to the probe before resetting itself. This command allows for remotely resetting the probe should a system error occur on it, however this only works provided the [RS-485](#) connection is still operational. Otherwise, the entire system will need to be powered off and on again to reset the probe. The reset on both microcontroller is triggered using software to setting the [System Reset Request \(SYSRESETREQ\)](#) bit in the [System Control Block \(SCB\)](#) register which triggers a system reset similar to that of pulling the reset pin low.

Chapter 6

Salinometer Evaluation and Testing

The [PCB](#) boards were delivered and tested. Some design errors were found which include using op-amps that were rated for 6V instead of 3V3, missing a connection between VDDA and VCC, and footprints errors with both the temperature sensor and depth sensor. The temperature sensor footprint was unable to be corrected, but the depth sensor could be corrected by flipping the depth sensor.

Once the circuitry was working and coded, the salinometer was tested. The testing was conducted in two phases. One phase before the probe was cast into epoxy resin and the other after the probe was cast into epoxy resin (section numbers?). A summary of these tests is shown in Table 6.1 and each test is discussed in further detail in the following sections.

The equipment used to verify these tests were a bench multimeter model Keysight U3401A which had voltage accuracy to 0.02% and resistance accuracy to 0.1%.

Table 6.1: A summary of the evaluation and testing of the salinometer.

| Sec. | Test Description | Result Metric | Ideal Result | Measured Results |
|------|---|----------------|--------------|-------------------|
| 6.1 | The minimum and maximum voltage output of the DAC between 0V and $V_{DD} = 3.3V$ | Range | 0 – 3.3V | 0 – 2.59V |
| 6.1 | The gain and offset of the output voltage of the DAC relative to the instructed voltage | Gain Offset | 1.0 0.0V | 0.9837 0.0070V |
| 6.2 | The gain and offset of the voltage measured by the ADC relative to the voltage measured by the multimeter | Gain Offset | 1.0 0.0V | 0.9877 0.0082V |
| 6.3 | The resistance of the calibration resistor R_{CAL} | Resistance | 5Ω | 5.00Ω |
| 6.4 | The gain and offset of the resistance measured by the salinometer relative to the resistance measured by the multimeter | Gain Offset | 1 0Ω | 1.0000 0.0000Ω |

6.1 DAC Voltage Range and Accuracy

The [DAC](#) configuration uses a transistor in order to buffer the [DAC](#) output which allows for the power draw to be support by the transistor instead of the [DAC](#). This is a common configuration where the [DAC](#) is connected to the non-inverting input of an op-amp whose output is connected to the base of an

6.1. DAC Voltage Range and Accuracy

NPN transistor. The emitter of the transistor is then connected to the inverting input of the op-amp which allows the buffered output to match the input of the **DAC**.

This configuration does have one disadvantage in that the output voltage of the **DAC** is limited by the transistor's V_{BE} such that the highest voltage output at the emitter of the transistor is $V_{DD} - V_{BE}$. According to the transistor's [data sheet](#), the buffered output should be limited to $3.3V - 0.6V = 2.7V$ when conducting $0A$ and $3.3V - 0.75V = 2.55V$ when conducting the maximum current of $33mA$ when the load is 100Ω . In order to assess the range and accuracy of the **DAC**, the **DAC** was instructed to output voltages from $0V$ to V_{DD} in intervals of 64-bits and the output voltage was measured at the base and emitter of the buffer transistor and under maximum load of 100Ω and no load. V_{DD} and GND were measured to be $3.299V$ and $0V$ respectively.

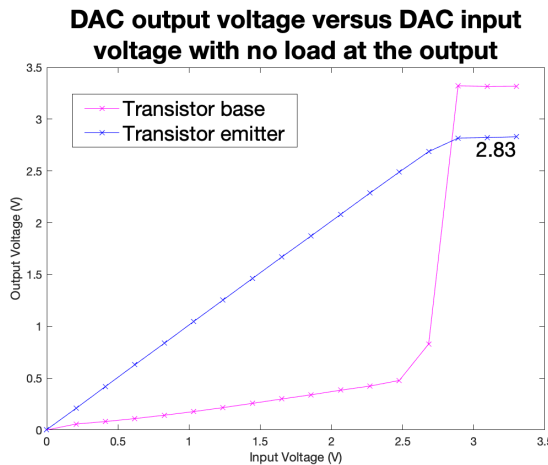


Figure 6.1: The input voltage versus the output voltage of the **DAC** with no load.

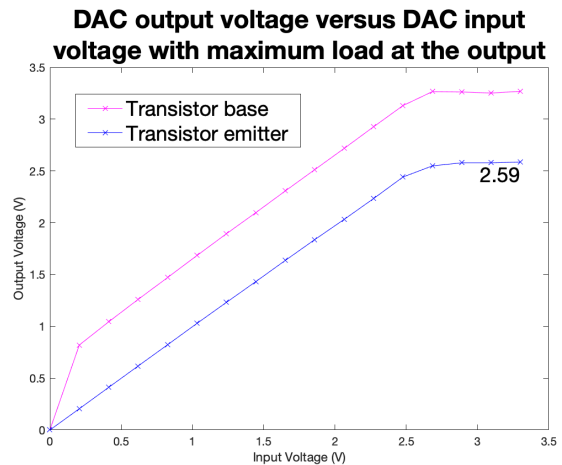


Figure 6.2: The input voltage versus the output voltage of the **DAC** with a load of 100Ω .

The results were graphed and are shown in Figure 6.1 and Figure 6.2. The voltage drop as a result V_{BE} can clearly be seen on Figure 6.2. The unloaded output voltage was able to reach $2.83V$ and the loaded output voltage was able to reach $2.59V$ which are slightly higher than the predicted limits.

An alternate attempt was also made to achieve a higher voltage output by using the internal reference voltage of the **DAC**. The internal reference voltage was set to $4 \times 1.21V = 4.84V$ and the **DAC** was instructed to output the maximum voltage. As expected, this was not able to increase the output voltage; the base of the transistor still outputted $3.3V$ and the emitter still outputted $2.83V$ while unloaded.

Due to the voltage limitations, the **DAC** will have a limited output in future testing and implementation to prevent the output voltage not reaching the desired input voltage. The output will be limited to $0V$ to $2.5V$ or 0 to 775 for fully loaded tests and the implementation and $0V$ to 2.7 or 0 to 837 for unloaded tests. When excluding the voltage readings above $2.5V$, the **DAC** was able to achieve a gain of $0.9837V/V$ and an offset $+0.0070V$ between the input voltage and output voltage when under maximum load.

6.2 ADC Accuracy

The [ADC](#) will be tested by measuring a range of voltages produced by the [DAC](#) and comparing the voltage measured by a multimeter to the voltage measured by the [ADC](#). The [ADC](#) will be configured in 12-bit mode with each measurement taking 15 [ADC](#) clock cycles and 5 measurements will be taken and averaged to increase the accuracy of the measurement. The accuracy of the [ADC](#) should ideally be 100%.

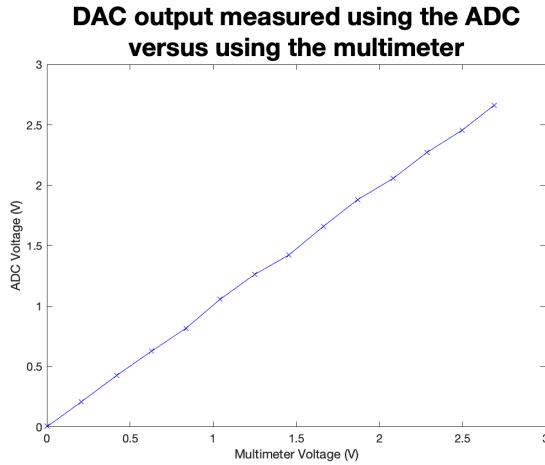


Figure 6.3: The voltage output by the [DAC](#) measured by a multimeter versus measured by the [ADC](#).

The results are shown in Figure 6.3. The [ADC](#) achieved a gain of $0.9877V/V$ and an offset of $0.0082V$ when compared to the multimeter.

6.3 Calibration Resistance

The calibration resistor will be measured by using the multimeter and by using the [ADC](#) with and without the gain applied. The calibration resistance was specified to be $5\Omega \pm 0.25\%$, and thus it is expected to be between 4.9875 and 5.0125Ω .

The calibration resistors were electrically disconnected, and the multimeter was used to measure the calibration resistor to be 5.25Ω when the probes where applied directly across one of the parallel calibration resistor's terminals. The multimeter cables measured 0.25Ω when connected to each other and thus the final resistance of the calibration resistor was 5.00Ω . It should be noted that the multimeter could only measure down to 0.01Ω and thus the true resistance could range from 4.99Ω to 5.01Ω .

6.4 Resistance Measuring Accuracy

The method of measuring resistance involves getting a voltage reading of the calibration resistor and a sample resistor which is attached between the titanium electrode ports. The resistance of the sample resistor is then calculated using the ratio between the voltage across the sample resistor and the calibration resistor.

This will be done using two methods: one with a single voltage from the [DAC](#) of $V_{DD}/2 = 1.65V$ and

one with voltage sweep from the **DAC** with 50 samples. It was noticed during the testing phase that low voltage readings were not accurate as single bit errors caused large changes in the resistance reading and thus the range of voltages will be limited to 0.3V to 2.6V or 93 to 806 bits. Both measurements will then be compared to the resistance measured by the multimeter. The range of the resistors used will be 0Ω to 10Ω as this is the expected range for the gold electrodes.

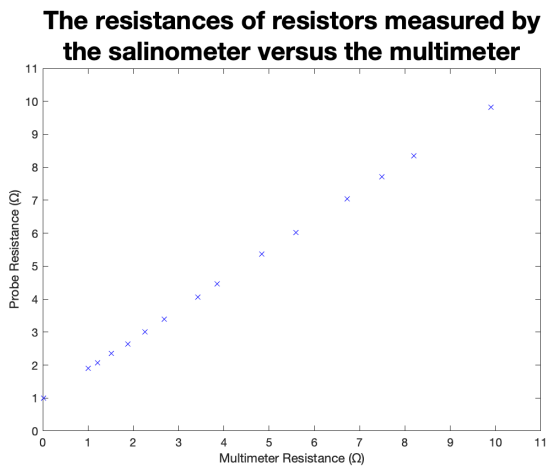


Figure 6.4: The resistance measuring test.

The resistances of resistors measured by the salinometer versus the multimeter using the corrected equation

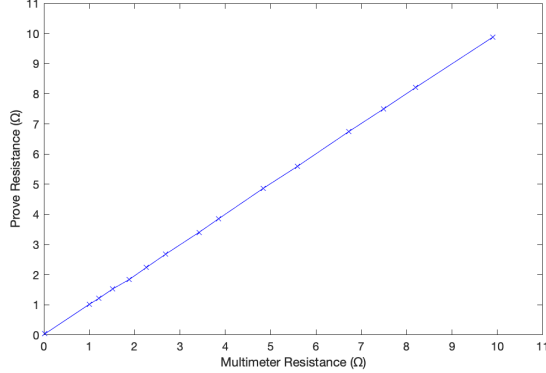


Figure 6.5: The resistance measuring test using the corrected equation.

The results are shown in Figure 6.4. The single voltage method and voltage sweep method were perfectly correlated with an r^2 value of 1.0000, however there was a clear error between the actual resistance and the resistance measured by the salinometer. This error was assumed to be due to the resistance of the switches and the traces. While these values could be measured and corrected for, a more efficient and arguably more accurate method would be to generate a curve of best fit and use this to correct the resistance readings.

In order to generate the equation of best fit, the voltage ratio Equation 5.1 is adjusted to include r_e which represents the resistance of the switches and traces as shown in Equation 6.1. The $R_{calibration}$, R_1 and r_e are condensed into the standard rational function coefficients p and q as shown in Equation ???. Finally, the equation is rearranged to give the resistance of the electrode in terms of the measured voltage ratio as shown in Equation 6.2.

$$\begin{aligned} V_{ratio} &= \frac{\frac{R_{electrode} + r_{e1}}{R_{electrode} + R_1 + r_{e2}}}{\frac{R_{calibration} + r_{e3}}{R_{calibration} + R_1 + r_{e4}}} \\ &= \frac{R_{electrode} + r_{e1}}{R_{electrode} + R_1 + r_{e2}} \times \frac{R_{calibration} + R_1 + r_{e4}}{R_{calibration} + r_{e3}} \end{aligned} \quad (6.1)$$

$$V_{ratio} = \frac{p_1 R_{electrode} + p_2}{R_{electrode} + q_1} \quad (6.2)$$

$$R_{electrode} = \frac{p_2 - q_1 V_{ratio}}{V_{ratio} - p_1} \quad (6.3)$$

The Equation 6.2 of best fit was confirmed using MATLAB giving $p_1 = 17.4687$, $p_2 = 18.4643$ and $q_1 = 91.8315$ with an r^2 value of 1.0000. The corrected resistance values were then obtained by applying Equation 6.3 to the voltage ratios and these results were graphed and are shown in Figure 6.5 with a gain of 1.0000 and an offset of 0.0000. Note that this correction equation is only valid when R_1 is 100Ω and separate equations will need to be generated should different values of R_1 be needed.

6.5 Linear Conductivity Measurement

This testing phase happened after the probe was cast into epoxy. The primary aim of this test is to discover if the salt water had a constant resistance for any given voltage. The testing procedure for all the below tests was to configure the probe's electrode, sample count, **DAC** voltage range and anything else that may prove useful to experiment with. A voltage sweep was then taken either forwards or backwards which was then sent over the **UART** connection to a computer where it was processed using Microsoft Excel and MATLAB to generate the graphs and metrics.

In addition to the results mentioned below, these tests also demonstrated that the **DAC** input, output and the calibration voltages were all linear. As mentioned above, in order to remove the linear gains of the op-amps, **DAC** and other components, only the ratio between the voltage across the electrodes and the calibration resistor voltage will be considered.

The first test aimed at discovering if the salt water had a linear resistance for any given voltage. This involved using the gold electrodes with the fringe shield to isolate any potential sources of non-linearities. These measurements were performed with both a forwards voltage sweep and a backwards voltage sweep. Each voltage step measurement was also taken in both directions as mentioned earlier. Ideally, these two measurements should be identical. However, they were clearly not as shown in Figure 6.6.

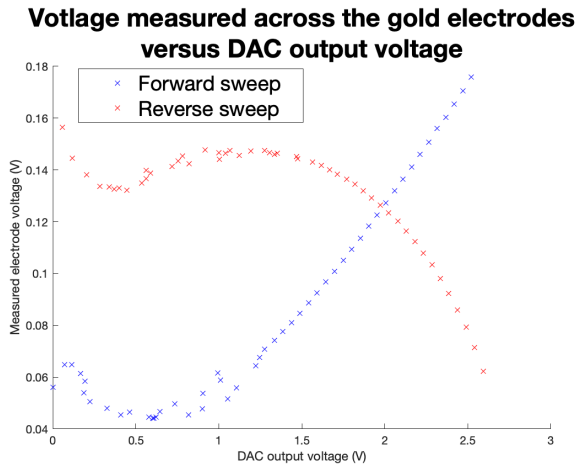


Figure 6.6: Conductivity test 1 with gold electrodes, the fringe shield, a voltage range of $0 - 2.6V$, and 50 samples taken of salt water sample of unknown .

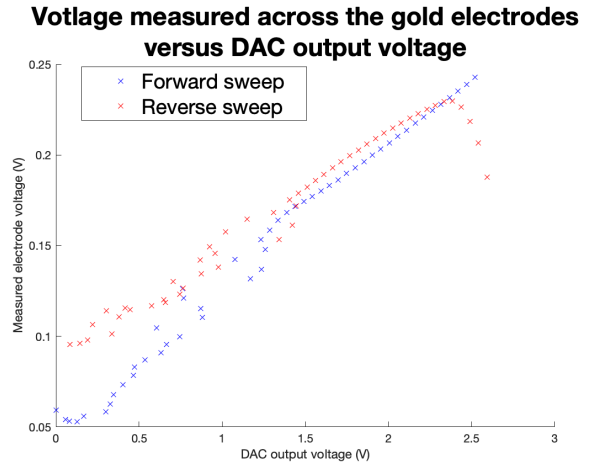


Figure 6.7: Conductivity test 2 with draining and resetting the **DAC** between each sample.

In order to isolate the reason for the inconsistency, multiple tests were conducted with adjustments made between each test. The first adjustment involved draining and resetting the **DAC** back to $0V$

each sample before it was set to the desired voltage. It should be noted that this added a small delay between each sample of around $10ms$. While this did make the forward and reverse sweeps more similar as shown in Figure 6.7, the initial voltage lag of the reverse sweep on the right-hand side of the graph was still present.

This result brought forward an alternative idea that the measurements of the water briefly altered its properties. This was unlikely to be a capacitive effect as the measurements were taken bidirectionally, and the capacitance would have been discharged. It was theorized that the alternative current through the water could be ionizing the dissolved material, ripping electrons free and allowing them to move more freely. However, this is purely speculative as the chemistry of the water is beyond the scope of this project and the knowledge of the author.

In order to further test this theory, the next test involved taking false, or priming, measurements at the maximum voltage before taking the actual measurements. This caused the measurements in both directions to start high and slowly move to their predicted paths, as shown in Figure 6.8, which further supports the theory that the measurements were affecting the water. This was further examined by using a varying number of priming measurements before conducting a reverse voltage sweep with 500 samples to accuracy track the voltage lag curve as shown in Figure 6.9. It should be noted that the voltage measurement effectively clips at $0.3V$ as the output of the $11\times$ gain op-amp reaches $0.3 \times 11 = 3.3V$ which is the maximum voltage of the ADC.

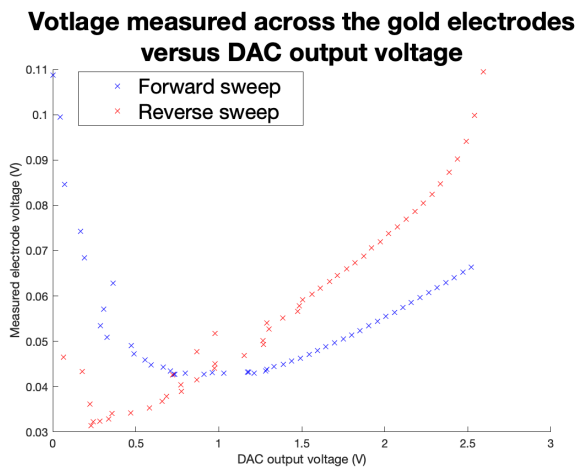


Figure 6.8: Conductivity test 3 with 25 priming measurements taken before the actual measurement.

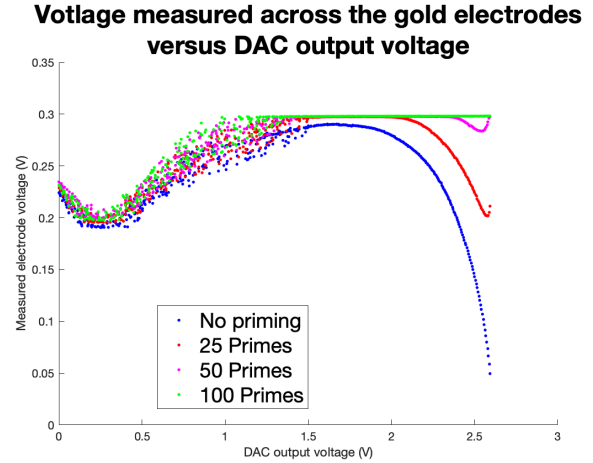


Figure 6.9: Conductivity test 4 with a varying number of priming measurements and all true measurement taken as reverse voltage sweeps with 500 samples.

This concluded that while there is a potential for the measurements to be perfectly primed, it is unlikely that the priming affect will have zero impact on the final measurements. It also indicates that the forward voltage sweeps could also be non-linear due to each subsequent measurement affecting the water before the next measurement is taken. Thus, an alternative method was needed to take the measurements. Since the priming effect on the forward voltage sweep decreased to join the expected curve, it was theorized that the water could relax from a primed state over a short enough period of time. More reasons needed here. The next tests involved waiting for the salt water to settle between

each measurement.

The first test involved waiting for 2s between each measurement and taking 50 samples. The relaxation waiting time happened while there was no voltage applied across the water.

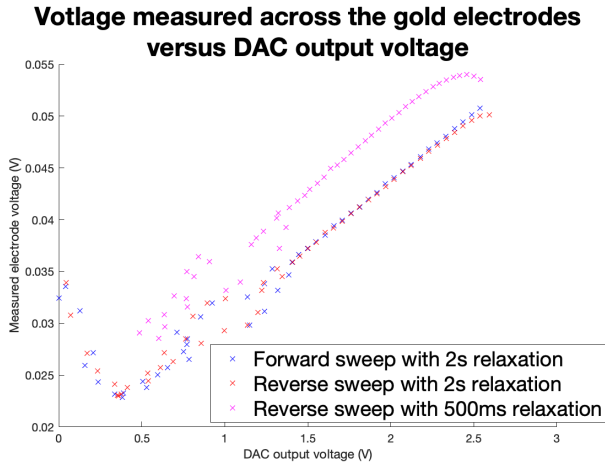


Figure 6.10: Conductivity test 5 with a varying amount of relaxation time before each measurement was taken and 50 samples.

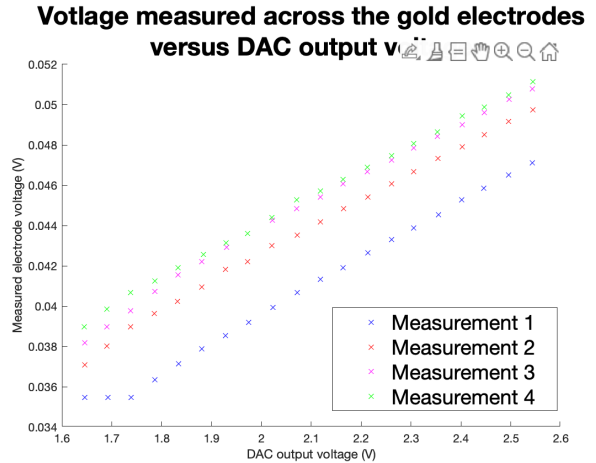


Figure 6.11: Conductivity test 6 with 4 identical tests of 20 samples with 2s of relaxation time between measurements.

Initial tests showed that the measurement was non-linear for au electrode however forwards and backwards voltage sweeps are not the same GRAPH this indicated that the measurement affected the voltage.

to isolate this it was thought that the dac might not be moving the voltage properly and thus the dac was reset and drained and then the voltage was pumped allowing for a longer time for the voltage to settle. this did not fix it. GRAPH

the next idea was to do false measurements at max voltage before doing sweeps. this caused the readings to start high and slowly move to the votlage sweep. GRAPH this shows that the measurement clearly affects the water by agitating it. this could be ionising the water, or polarising it or another affected

the next test involved letting it settle between each measurement as in theory this would cause. starting at 2s. this gave two graphs that matched perfecetly for the forward and backwards sweep. GRAPH

waiting 2s per measurement for 50 samples took very long and an alternate method was to change the water infront of the electrodes by agitating/stirring the water. this gave repeatable results that also showed a difference between two different water samples. GRAPH taking fewer samples over the more linear voltage range gave something that was approximately linear.

trying to find a decernable metric from these graphs by analysing $A/(s+p)$ between two samples of arbitrary salinity. TABLE

try repeated single measurements.

ac testing not rigged up correctly. GRAPH

Chapter 7

Conclusions

The purpose of this project was to...

This report began with...

The literature review was followed in Chapter...

The bulk of the work for this project followed next, in Chapter...

In Chapter...

Finally, Chapter... attempted to...

In summary, the project achieved the goals that were set out, by designing and demonstrating...

Chapter 8

Recommendations

Bibliography

- [1] *The Influence Of Formation Anisotropy Upon Resistivity - Porosity Relationships*, ser. SPWLA Annual Logging Symposium, vol. All Days, 06 1981.
- [2] “Mapping salty waters,” 2019. [Online]. Available: https://www.esa.int/Applications/Observing_the_Earth/Space_for_our_climate/Mapping_salty_waters
- [3] J. Jonsson, K. Smedfors, L. Nyholm, and G. Thornell, “Towards chip-based salinity measurements for small submersibles and biologgers,” *International Journal of Oceanography*, vol. 2013, p. 11, 2013. [Online]. Available: <http://dx.doi.org/10.1155/2013/529674>
- [4] N. Snow and I. D. C. (NSIDC), “Ice sheet quick facts,” 2024. [Online]. Available: <https://nsidc.org/learn/parts-cryosphere/ice-sheets/ice-sheet-quick-facts>
- [5] R. H. Stewart, *Introduction to Physical Oceanography*. Texas A&M University Press, 2004. [Online]. Available: <https://www.uv.es/hegogui/Kasper/por%20Robert%20H%20Stewart.pdf>
- [6] R. F. HU Sverdrup, MW Johnson, *The Oceans, Their Physics, Chemistry, and General Biology*. New York: Prentice-Hall, 1942. [Online]. Available: <http://ark.edlib.org/ark:/13030/kt167nb66r/>
- [7] E. L. Lewis and R. G. Perkin, “Salinity: Its definition and calculation,” *Journal of Geophysical Research*, vol. 83, no. C1, pp. 466–478, 1978. [Online]. Available: <https://agupubs.onlinelibrary.wiley.com/doi/epdf/10.1029/JC083iC01p00466>
- [8] Y. Zheng, Y. Liu, J. Zhou, and Y. Wang, “Electrical conductivity of the global ocean,” *Earth, Planets and Space*, vol. 69, no. 1, pp. 1–10, 2017.
- [9] I. O. Commission, “Teos-10: The international thermodynamic equation of seawater (teos-10) for temperature, salinity, density, sound speed, and other oceanographic variables,” *Manuals and Guides*, vol. 56, 2010. [Online]. Available: https://www.teos-10.org/pubs/TEOS-10_Manual.pdf
- [10] E. B. editors, “Seawater,” *Encyclopædia Britannica*, 2024. [Online]. Available: <https://www.britannica.com/science/seawater>
- [11] W. S. Wooster, A. J. Lee, and G. Dietrich, “Redefinition of salinity,” *Journal of Marine Research*, vol. 27, no. 3, 1969.
- [12] S. Scientific, “How accurate is salinity measured by my ctd? what factors impact accuracy.” [Online]. Available: <https://blog.seabird.com/ufaqs/how-accurate-is-salinity-measured-by-my-ctd-what-factors-impact-accuracy/>
- [13] U. G. Survey, “Water density,” 2018. [Online]. Available: [https://www.usgs.gov/special-topics/water-science-school/science/water-density#:~:text=A%20common%20unit%20of%20measurement,Celsius%20\(39.2%20Fahrenheit\).](https://www.usgs.gov/special-topics/water-science-school/science/water-density#:~:text=A%20common%20unit%20of%20measurement,Celsius%20(39.2%20Fahrenheit).)

- [14] B. Kjerfve, "Measurement and analysis of water current, temperature, salinity, and density," in *Estuarine hydrography and sedimentation*, K. Dyer, Ed. Cambridge: Cambridge University Press, 1983, pp. 187–226.
- [15] U. of Washington Department of Oceanography, "A compilation of articles reporting research," 1966.
- [16] F. J. Millero and A. Poisson, "International one-atmosphere equation of state of seawater," *Deep Sea Research Part A. Oceanographic Research Papers*, vol. 28, no. 6, pp. 625–629, 1981. [Online]. Available: <https://www.sciencedirect.com/science/article/pii/0198014981901229>
- [17] H. Schmidt, S. Seitz, E. Hassel, and H. Wolf, "The density–salinity relation of standard seawater," *Ocean Science*, vol. 14, no. 1, pp. 15–40, 2018. [Online]. Available: <https://os.copernicus.org/articles/14/15/2018/>
- [18] C. T. Swift and R. E. McIntosh, "Considerations for microwave remote sensing of ocean-surface salinity," *IEEE Transactions on Geoscience and Remote Sensing*, vol. GE-21, no. 4, pp. 480–491, 1983.
- [19] C. Gabarró, J. Font, A. Camps, M. Vall-llossera, and A. Julià, "A new empirical model of sea surface microwave emissivity for salinity remote sensing," *Geophysical Research Letters*, vol. 31, no. 1, 2004. [Online]. Available: <https://agupubs.onlinelibrary.wiley.com/doi/abs/10.1029/2003GL018964>
- [20] S. Yueh, R. West, W. Wilson, F. Li, E. Njoku, and Y. Rahmat-Samii, "Error sources and feasibility for microwave remote sensing of ocean surface salinity," *IEEE Transactions on Geoscience and Remote Sensing*, vol. 39, no. 5, pp. 1049–1060, 2001.
- [21] R. Millard and G. Seaver, "An index of refraction algorithm for seawater over temperature, pressure, salinity, density, and wavelength," *Deep Sea Research Part A. Oceanographic Research Papers*, vol. 37, no. 12, pp. 1909–1926, 1990. [Online]. Available: <https://www.sciencedirect.com/science/article/pii/019801499090086B>
- [22] D. Malardé, Z. Y. Wu, P. Gross, J.-L. de Bougrenet de la Tocnaye, and M. L. Menn, "High-resolution and compact refractometer for salinity measurements," *Measurement Science and Technology*, vol. 20, no. 1, p. 015204, dec 2008. [Online]. Available: <https://dx.doi.org/10.1088/0957-0233/20/1/015204>
- [23] O. A. Tengesdal, "Measurement of seawater refractive index and salinity by means of optical refraction," Master's thesis, University of Bergen, 2012.
- [24] Y. Liao, K. Yang, and X. Shi, "Theoretical study on simultaneous measurement of seawater temperature and salinity based on dual fiber interferometers combined with nonlinear decoupling algorithm," *Measurement*, vol. 211, p. 112596, 2023. [Online]. Available: <https://www.sciencedirect.com/science/article/pii/S0263224123001604>
- [25] S. Yang, J. Xu, L. Ji, Q. Sun, M. Zhang, S. Zhao, and C. Wu, "In situ measurement of deep-sea salinity using optical salinometer based on michelson interferometer,"

- Journal of Marine Science and Engineering*, vol. 12, no. 9, 2024. [Online]. Available: <https://www.mdpi.com/2077-1312/12/9/1569>
- [26] G. R. C. Possetti, R. C. Kamikawachi, C. L. Prevedello, M. Muller, and J. L. Fabris, “Salinity measurement in water environment with a long period grating based interferometer,” *Measurement Science and Technology*, vol. 20, no. 3, p. 034003, feb 2009. [Online]. Available: <https://dx.doi.org/10.1088/0957-0233/20/3/034003>
- [27] L. V. Nguyen, M. Vasiliev, and K. Alameh, “Three-wave fiber fabry-pérot interferometer for simultaneous measurement of temperature and water salinity of seawater,” *IEEE Photonics Technology Letters*, vol. 23, no. 7, pp. 450–452, 2011.
- [28] Y. Zhao, J. Zhao, Y. Peng, R.-J. Tong, and L. Cai, “Simultaneous measurement of seawater salinity and temperature with composite fiber-optic interferometer,” *IEEE Transactions on Instrumentation and Measurement*, vol. 71, pp. 1–8, 2022.
- [29] R. Somaraju and J. Trumpf, “Frequency, temperature and salinity variation of the permittivity of seawater,” *IEEE Transactions on Antennas and Propagation*, vol. 54, no. 11, pp. 3441–3448, 2006.
- [30] O. A. Tengesdal, B. L. Hauge, and L. E. Helseth, “Electromagnetic and optical methods for measurements of salt concentration of water,” *Journal of Electromagnetic Analysis and Applications*, vol. 6, no. 6, 2014.
- [31] R. Benjankar and R. Kafle, “Salt concentration measurement using re-usable electric conductivity-based sensors,” *Water Air and Soil Pollution*, vol. 232, no. 13, p. 13, 2021. [Online]. Available: <https://doi.org/10.1007/s11270-020-04971-7>
- [32] “Water salinity-meter : 7 steps.” [Online]. Available: <https://www.instructables.com/Water-Salinity-meter/>
- [33] S.-B. Scientific, “Conversion of pressure to depth,” 2024. [Online]. Available: <https://www.google.com/url?sa=t&rct=j&q=&esrc=s&source=web&cd=&ved=2ahUKEwij6ebU1sCIAxXPiv0HHXDELasQFnoECCMQAQ&url=https%3A%2F%2Fwww.seabird.com%2Fasset-get.download.jsa%3Fid%3D54627861710&usg=AOvVaw1fK2h9jmgpiBuyu8lkM1tl&opi=89978449>
- [34] T. L. Hill, *An introduction to statistical thermodynamics*. Courier Corporation, 1986.
- [35] A. Poisson and M. H. Gadhoumi, “An extension of the practical salinity scale 1978 and the equation of state 1980 to high salinities,” *Deep Sea Research Part I: Oceanographic Research Papers*, vol. 40, no. 8, pp. 1689–1698, 1993. [Online]. Available: <https://www.sciencedirect.com/science/article/pii/096706379390022U>
- [36] G. T. Furukawa, J. L. Riddle, and W. R. Bigge, “The international practical temperature scale of 1968 in the region 13.81 k to 90.188 k as maintained at the national bureau of standards,” *Journal of Research of the National Bureau of Standards-A. Physics and Chemistry*, vol. 77A, no. 3, pp. 309–322, 1973. [Online]. Available: https://nvlpubs.nist.gov/nistpubs/jres/77A/jresv77An3p309_A1b.pdf

- [37] H. Preston-Thomas, “The international temperature scale of 1990 (its-90),” *Metrologia*, vol. 27, no. 107, pp. 3–10, 1990. [Online]. Available: https://www.nist.gov/system/files/documents/pml/div685/grp01/ITS-90_metrologia.pdf
- [38] M. Solomentsev and A. J. Hanson, “Modeling current distribution within conductors and between parallel conductors in high-frequency magnetics,” *IEEE Open Journal of Power Electronics*, vol. 3, pp. 635–650, 2022.
- [39] S. Hwang and J. Shim, “A method for current spreading analysis and electrode pattern design in light-emitting diodes,” *IEEE Transactions on Electron Devices*, vol. 55, no. 5, pp. 1123–1128, 2008.
- [40] S.-R. Jeon, Y.-H. Song, H.-J. Jang, G. M. Yang, S. W. Hwang, and S. J. Son, “Lateral current spreading in GaN-based light-emitting diodes utilizing tunnel contact junctions,” *Applied Physics Letters*, vol. 78, no. 21, pp. 3265–3267, 05 2001. [Online]. Available: <https://doi.org/10.1063/1.1374483>
- [41] Jason, “Current spreading in long objects,” 7515 Colshire Drive, McLean, Virginia 22102-753, oct 2008, approved for public release; distribution unlimited.
- [42] “What is the typical water conductivity range? | atlas scientific,” 2022. [Online]. Available: <https://www.atlascientific.com/blog/2022/09/water-conductivity-range>
- [43] F. Walsh, “Electrode reactions in metal finishing,” *Transactions of the Institute of Metal Finishing*, vol. 69, pp. 107–111, 08 1991.
- [44] M. Hegg and A. Maminshev, “Influence of variable plate separation on fringing electric fields in parallel-plate capacitors,” in *Conference Record of the 2004 IEEE International Symposium on Electrical Insulation*, 2004, pp. 384–387.
- [45] G. J. Sloggett, N. G. Barton, and S. J. Spencer, “Fringing fields in disc capacitors,” *Journal of Physics A: Mathematical and General*, vol. 19, no. 14, p. 2725, oct 1986. [Online]. Available: <https://dx.doi.org/10.1088/0305-4470/19/14/012>